Inorganic Chemistry

ARTICLE

pubs.acs.org/IC

QM and QM/MM Studies of Uranyl Fluorides in the Gas and Aqueous Phases and in the Hydrophobic Cavities of Tetrabrachion

Samuel O. Odoh, Sean M. Walker, Markus Meier, Jörg Stetefeld, and Georg Schreckenbach*

Department of Chemistry, University of Manitoba, Winnipeg, Manitoba, Canada R3T 2N2

Supporting Information

ABSTRACT: The structural properties and electronic structures of penta-coordinated uranyl complexes belonging to the $[UO_2F_n(H_2O)_{5-n}]^{2-n}$ series have been studied in the gas and aqueous phases using density functionals with relativistic pseudopotentials and all-electron basis sets in the gas-phase calculations in combination with COSMO in the aqueous phase. In addition, the conformational orientation and structural and electronic properties of $[UO_2F_5]^{3-}$ in the hydrophobic cavities of the right-handed coiled-coil (RHCC) protein of tetrabrachion have been determined using the hybrid QM/MM method. Although there is good agreement between the available experimental geometrical parameters and the values obtained in the aqueous phase using pseudopotentials or all-electron basis sets, variation of the uranyl U═O bond with the number of fluoride ligands is only truly captured after the inclusion of five water molecules in the second coordination sphere around the molecules. The docking procedure used in this work shows that there are only two possible orientations of the uranyl group of $[UO_2F_5]^{3-}$ embedded in the hydrophobic cavities of the RHCC protein. The two orientations are exclusively along the axes perpendicular to the protein axial channel with no possible orientation of the uranyl group along the axial channel because of both steric effects and interaction with the alkyl chain of the isoleucine residues pointing into the axial channel. In addition, the embedded complex is always positioned nearer to the isoleucine residues at the N-terminal ends of the hydrophobic cavities. Energy analysis, however, reveals that both conformations can only be observed in cavity 2, the largest hydrophobic cavity. The structural and electronic properties of the ligand embedded in this cavity are very similar to those of the gas-phase structure. A comparable study of $[Pt(CN)_6]^{2-}$ and the anticancer drug cisplatin, $[PtCl_2(NH_3)_2]$, in cavity 2, revealed the existence of just two orientations for the former, similar to the uranyl complex, and multiple orientations for the latter.

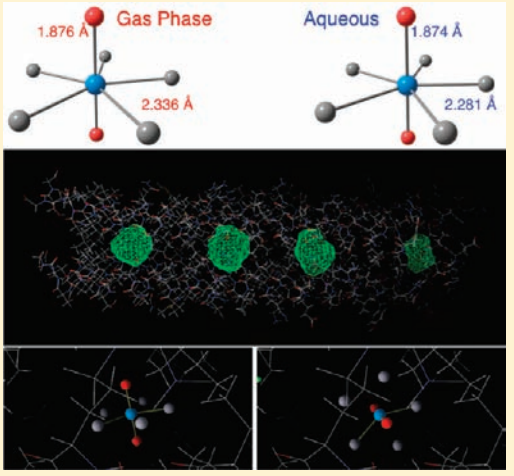

INTRODUCTION

The tetrabrachion complex of archaebacterium *Staphylothermus marinus* has been shown to contain a right-handed coiled-coil (RHCC) protein.[1−5] The thermodynamically stable RHCC contains four parallel α-helical chains oriented in a right-handed fashion with four hydrophobic cavities aligned along the axis of the protein (Figure 1). In the native crystal structure, the largest hydrophobic cavity of tetrabrachion contains nine water molecules aggregated into a cluster, while the other cavities contain five, one, and two water molecules, respectively, according to their sizes. The aggregation of the water molecules in the cavities of tetrabrachion is due to the exclusively aliphatic and hydrophobic lining of the cavity walls. Yin et al. have shown that metastable water complexes held together by hydrogen bonds exist in the largest cavity of RHCC at both room (298 K) and high (365 K) temperatures.[6,7] They also demonstrated the existence of significant entropic contributions to the thermodynamics of the filling of the largest hydrophobic cavity by multiple water molecules.

A recent review on the nature and structure of coiled-coil proteins as well as their potential use for therapeutic purposes has been published by McFarlane and co-workers.[8] The presence of large cavities in such proteins and the ability of these cavities to bind or hold cargo molecules make them ideal drug-delivery vehicles. Modification of the terminal amino acids of coiled coils with specific labeling groups can be used for specific drug targeting, thus reducing the overall cytotoxicity of a therapeutic molecule. Perhaps the most important potential use of coiled-coil proteins is for the delivery of cancer drugs to tumor cells. In fact, the ability of the RHCC of tetrabrachion to incorporate and transfer cisplatin, $[PtCl_2(NH_3)_2]$, into mammalian cells has been studied by Eriksson et al.[2] They found that RHCC stably incorporates cisplatin at room temperature and that the RHCC-cisplatin complex (RHCC-C) rather efficiently binds to cells. The RHCC-C complex was found to be equally or sometimes more effective against cancer cells as the pure cisplatin

Received: January 24, 2011
Published: March 10, 2011

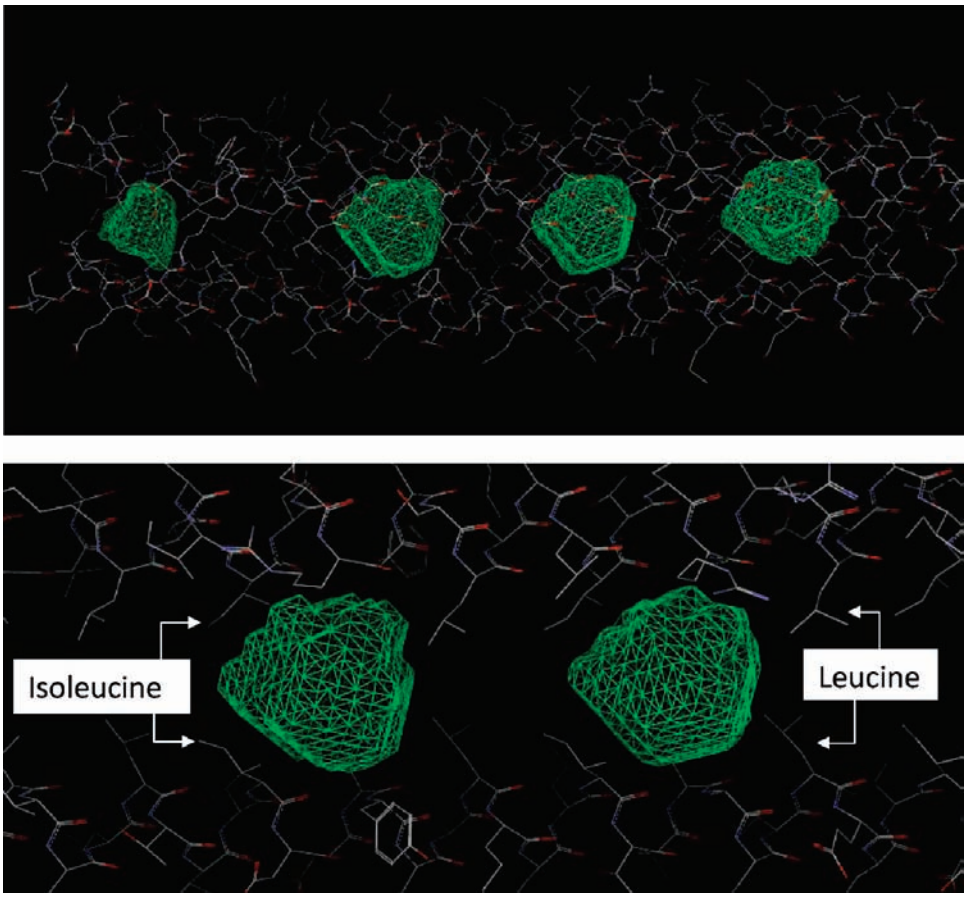

Figure 1. Top: RHCC protein of tetrabrachion. Cavities 1−4 from the N terminus (left) to the C terminus (right) are shown. Bottom: Two monomer chains of the RHCC tetramer. Isoleucine and leucine side chains are found at the N-terminal and C-terminal ends, respectively, of cavities 2 and 3.

drug. Their work raises the possibility of the RHCC protein being used as a carrier for cisplatin in therapeutic usage. However, an obstacle to the long-term goal of using the RHCC as a drug-delivery vehicle is the issue of diseased cell targeting. Theoretical studies of cisplatin in the cavities of the RHCC could potentially be used in the design of modifications to either the cargo molecule or the aliphatic chains lining the cavities.

Moreover, cancer drugs are not the only kind of molecular systems that can be embedded in the hydrophobic cavities of RHCC. Indeed, several heavy metals and their compounds were incorporated into the cavities of the RHCC tetrabrachion during X-ray crystallographic studies of its structure.[5] It would thus appear that the hydrophobic cavities are filled with water clusters in the native structure, while the occupying water clusters are displaced by any compact molecular or ionic system present in solution. The displacement of water clusters embedded in the hydrophobic cavities by a single ionic complex will be favored by an increase in the total entropy, which will dominate the positive-leaning enthalpy of transferring ionic or hydrophilic species from the polar aqueous solvent into a cavity lined exclusively with aliphatic side chains.[6,7]

Actinide complexes like uranyl fluoride used in the determination of the phase information of the RHCC are also incorporated into the hydrophobic cavities.[4,5,9,10] Uranyl fluorides have been extensively studied theoretically and experimentally in both the gas and aqueous phases.[11−26] The hydrophobic cavities of the RHCC of tetrabrachion represent a rather unique and "different" environment in which to study the structure and bonding of uranyl fluorides. The extent to which the wave function of a cargo molecule is perturbed by the protein environment can be determined by comparing the geometrical and electronic structures of uranyl fluorides in the hydrophobic cavities of RHCC, in the gas phase and in solution. In addition, because the cavities of the RHCC are nonpolar, it will be interesting to see if there is any "local order" (or favored orientations) to the alignment of polar molecules like uranyl fluoride.

Full quantum mechanical (QM) calculations on the protein-actinide species complex are currently very computationally expensive not in the least because of the large number of degrees of freedom in the protein.[27] Indeed, the large number of loose degrees of freedom in biological macromolecules makes the concept of a "global or local" structural minimum less important than that in stiff molecules, and hence the need for the selection of a probabilistic ensemble corresponding to all possible configurations in which the macromolecule could exist at a certain temperature.[27] The quantum mechanical/molecular mechanics (QM/MM) method is a hybrid method in which the active or interesting site is treated with computationally more demanding QM methods, while the remainder of the system (remainder of the macromolecule and/or environmental water) is treated classically using molecular mechanics (MM).[28−42] This method has been used extensively in literature to study large systems and represents a balance between the accuracy of full QM treatment and the computational efficiency of a full classical treatment using MM.[43−46]

dx.doi.org/10.1021/ic2001706 |*Inorg. Chem.* 2011, 50, 3141–3152

There have been very few theoretical studies of actinide complexes using the QM/MM method. Infante et al. studied the nature of the water solvation shells around both the tetrafluoro and tetrahydroxo complexes of the uranyl dication.[15,16,47,48] The solvent water molecules were treated with MM, while the uranyl complexes were treated with density functional theory (DFT) with relativistic effects included using the zeroth-order regular approximation, ZORA.[49−51] The interaction between the solvent water MM region and the wave function of the actinide complex QM region was restricted to mechanical coupling. A comparison of the results of the QM/MM calculations with those obtained with full QM calculations indicated qualitative and some quantitative agreements in the computed geometric and electronic properties.

Here we present QM/MM simulation studies on uranyl pentafluoride, $[UO_2F_5]^{3-}$, incorporated in the hydrophobic cavities of the RHCC using DFT with relativistic effective core potentials (RECPs) to include relativistic effects on the QM region while classically representing the RHCC using the popular AMBER95 force field.[52] Electrostatic coupling of the MM charges to the wave function of the QM region and other nonbonded interactions like van der Waals (vdW) and electrostatic interactions are included in the calculations. The structural and electronic properties of $[UO_2F_5]^{3-}$ in the hydrophobic cavities are compared to those in both the gas and aqueous phases. The presence of favored configurations for the embedded actinide complex with respect to the axial channel of the protein is reliably proven using the QM/MM method. This is in agreement with preliminary experimental evidence for the existence of two orientations for uranyl fluoride in the largest hydrophobic cavity of the RHCC.[53] Finally, the incorporation of the anticancer drug, cisplatin, and $[Pt(CN)_6]^{2-}$ into the largest hydrophobic cavity is examined using the same methodology as that used for uranyl fluoride. It should be fully noted that current theoretical calculations of cisplatin in the hydrophobic cavities were stimulated by the possibility of therapeutic use, while similar work on $[UO_2F_5]^{3-}$ in these cavities was motivated by structural and electronic considerations (the presence of local order in the arrangement of this molecule in the cavities and the effect of the cavity walls on the electronic structure of the actinide complex). The common theme connecting the two subjects (cisplatin and uranyl complexes) is provided in the common protein environment with its unique cavity structure and the resulting application of a common methodology. There is undoubtedly little therapeutic potential for this actinide complex.

The remainder of this report is organized as follows. The computational calculations carried out are first described, followed by a discussion of the geometric and electronic structures of uranyl fluorides in the gas and aqueous phases. The chemistry of uranyl fluorides in the hydrophobic cavities of tetrabrachion is then described using $[UO_2F_5]^{3-}$ as a representative complex. Finally, we compare the incorporation of $[UO_2F_5]^{3-}$ in the hydrophobic cavities to that of other ligands such as cisplatin and $[Pt(CN)_6]^{2-}$.

COMPUTATIONAL DETAILS

The molecular geometries of all members of the $[UO_2F_n(H_2O)_{5-n}]^{2-n}$ series and cisplatin were optimized in the gas and aqueous phases using the B3LYP[54−57] and BP86[57,58] functionals. The uranium and platinum atoms were described with the Stuttgart small-core (60 core electrons represented by a pseudopotential) RECP and associated valence basis sets, while all other atoms were described with the 6-311++G** basis set.[59−61] All g functions in the valence basis set associated with the Stuttgart pseudopotentials were removed. In addition, a set of diffuse f-type basis functions ($\alpha = 0.005$) was added to allow for an accurate description of the lowest unoccupied molecular orbitals of the uranyl complexes. All of the RECP calculations were carried out in the NWChem 5.1.1 package.[62,63] The aqueous-phase calculations employed the conductor-like screening solvation model (COSMO).[64,65] The atomic radii used in forming solvation cavities around the molecules in these calculations are 2.18, 1.72, 1.72, and 1.30 Å for the uranium, fluorine, oxygen, and hydrogen atoms, respectively.

Also, the ZORA relativistic approach[49−51] with triple-ξ-polarized (TZP) all-electron basis sets and the BP86 functional was used in the optimization of the geometries of all of the molecules. No core atomic orbitals were frozen. These ZORA-DFT calculations were carried out using the Amsterdam Density Functional (ADF 2009) package with an integration parameter of 6.0.[66−68] Multipole-derived atomic charges, Mayer bond orders, and Mulliken atomic charges were obtained from these all-electron calculations.[69] In ADF,[70] the aqueous-phase calculations were carried out using COSMO[64,65] and atomic radii identical with those used in the RECP calculations were employed. Modern approaches in the theoretical calculations of actinide chemistry in the gas and aqueous phases have recently been reviewed.[71]

The starting configurations for the QM/MM simulations of $[UO_2F_5]^{3-}$, $[Pt(CN)_6]^{2-}$, and cisplatin encapsulated in the hydrophobic cavities of the RHCC were generated using *AutoDock*.[72] The water clusters, $(H_2O)_n$ (where n = 9, 5, 1, and 2 for the largest, second-largest, third-largest, and smallest cavities, respectively), in the cavities were evacuated prior to docking.[5] Ligand-optimized geometries and multipole-derived atomic charges obtained from the BP86/ZORA/TZP calculations were used in the docking. The vdW parameters used for the uranium atom were taken from the work of Guilbaud and Wipff.[73] The parameters used for platinum atoms when cisplatin was docked in the cavity were obtained from the work of Spiegel et al.[74] The hydrophobic cavities or binding sites for the ligands were determined from the amino acid sequence of the X-ray structure[3] and confirmed using various grids in *AutoDock*. The simulated annealing algorithm was used to generate structures, which were then clustered and ranked by their energies. Several initial temperatures for the annealing were tried in addition to using 25, 50, and 75 cooling runs.

The atoms of the RHCC protein and crystal waters were represented with the AMBER95 force field in the QM/MM calculations.[52] The QM/MM calculations were performed using the NWChem 5.1.1 and 6.0 codes.[62,63] There was no necessity for link atoms because there are no formal bonds between the embedded molecules and the cavity walls of the protein. DFT calculations using the BP86 functional as well as the Stuttgart small-core RECPs for the uranium and platinum atoms and the 6-311++G** basis set for all other atoms were performed on the embedded molecules.[61] The cutoff for all nonbonded interactions was set at 15 Å. The ligands considered in this work are $[UO_2F_5]^{3-}$ and cisplatin embedded in the protein hydrophobic cavities. Electrostatic coupling (polarization of the wave function of the QM region by the charges of the neighboring MM atoms), Coulombic electrostatic, and vdW interactions of the protein and ligand atoms were included in the calculations. The geometry optimization procedure included the sequential optimization of both the embedded ligands (QM) and the RHCC protein (MM) until energy convergence (5.0×10^{-5} hartree) was attained. The vibrational frequencies of the embedded ligands were also determined after geometry optimization by numerical differentiation. All of the MM atoms were held frozen during the finite-difference vibrational calculations.

RESULTS AND DISCUSSION

$[UO_2F_n(H_2O)_{5-n}]^{2-n}$ Complexes: Gas and Aqueous Phases. The structural parameters and uranyl vibrational

dx.doi.org/10.1021/ic2001706 |*Inorg. Chem.* 2011, 50, 3141–3152

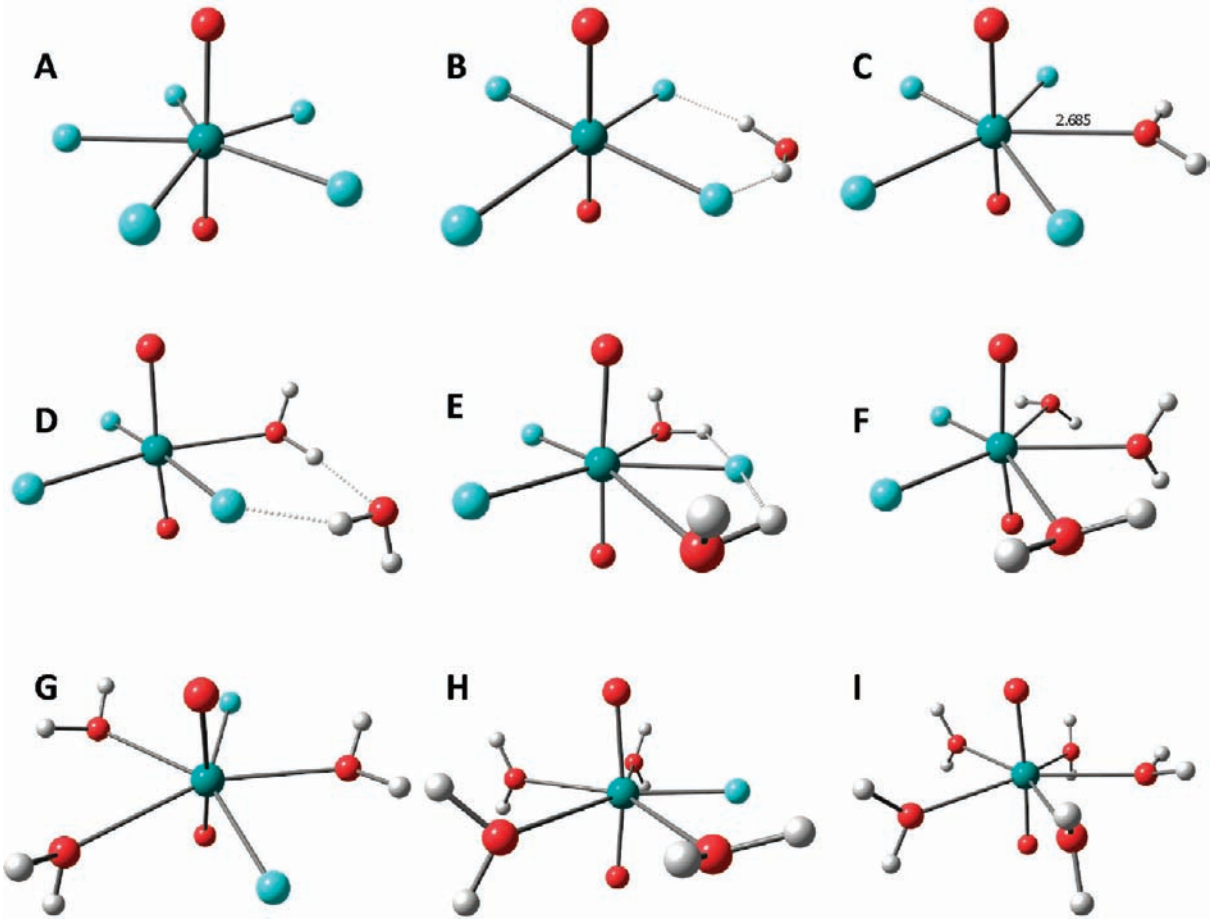

Figure 2. Aqueous-phase structures of the $[UO_2F_n(H_2O)_{5-n}]^{2-n}$ complexes optimized at the BP86/TZP/ZORA/COSMO level: (A) $[UO_2F_5]^{3-}$, (B) $[UO_2(H_2O)F_4]^{2-}$ structure 1, (C) $[UO_2(H_2O)F_4]^{2-}$ structure 2, (D) $[UO_2(H_2O)_2F_3]^{-}$ structure 1, (E) $[UO_2(H_2O)_2F_3]^{-}$ structure 2, (F) $[UO_2(H_2O)_3F_2]^{0}$ structure 1, (G) $[UO_2(H_2O)_3F_2]^{0}$ structure 2, (H) $[UO_2(H_2O)_4F]^{+}$, and (I) $[UO_2(H_2O)_5]^{2+}$.

stretching frequencies of the $[UO_2F_n(H_2O)_{5-n}]^{2-n}$ compounds (Figure 2) obtained using DFT with the small-core RECP and all-electron ZORA approaches are given in Table 1. Methodologically, the U═O bond lengths computed using the B3LYP hybrid functional are generally shorter than those obtained with the BP86 functional. This is in agreement with literature experience and is reflected in the larger wavenumbers of the uranyl symmetric and asymmetric stretching vibrations obtained with the hybrid functional (Table 1).[21,75−77] Also, given a comparable basis set size and the same density functional, nearly identical bond lengths and vibrational frequencies are obtained from both the RECP and all-electron ZORA approaches (Table 1). This agrees with recent estimates that the bond lengths obtained with small-core RECPs are in very good agreement with those obtained using an all-electron four-component relativistic approach, while the calculated vibrational wavenumbers are lower than the all-electron basis set results.[21,75]

There is a gradual increase in the calculated U═O and U−F bond lengths as the number of fluoride ligands is increased down the $[UO_2F_n(H_2O)_{5-n}]^{2-n}$ series (Table 1). This is especially true for conformers in which the five ligands are in the first coordination sphere about the equatorial plane. The calculated Mayer bond orders of the U═O bonds in the complexes are presented in Table 2. Concomitant with the increasing U═O bond lengths, there is a decrease in the calculated U═O bond order as the number of fluoride ligands in the complexes is increased. This lengthening of the U═O bond is accompanied by a decrease in the calculated Mulliken charges on both the uranium atom and the uranyl group (Figure 3 and Table 2). On the basis of the calculated Mayer bond orders and atomic charges in the molecules, an additive-ionic Lewis base effect of multiple fluoride ligands could be used as an explanation for the increasing U−F bonds lengths[13] even as such an approach can be used to explain the increase in the U═O and U−OH_2 bond lengths.

The sequential-average ligand binding energies (BEs) of the uranyl complexes provide an alternative way of examining the effect of a greater number of fluoride ligands. The ligand BE, $\Delta E_{binding}$, to the uranyl moiety of a $[UO_2F_n(H_2O)_{5-n}]^{2-n}$ complex is given by $E_{complex} - E_{uranyl} - nE_{fluoride\ ion} - (5 - n)E_{water}$. The difference between the ligand BEs of successive members of the $[UO_2F_n(H_2O)_{5-n}]^{2-n}$ series represents the average energy required for the sequential replacement of an aquo ligand by a fluoride ion. The average ligand BEs calculated for the $[UO_2F_n(H_2O)_{5-n}]^{2-n}$ complexes in solution increases as the number of fluoride ligands increases (Table 2). This is to be expected given the replacement of a neutral aquo ligand coordinated to the uranyl cation by an anionic fluoride ligand. However, the calculated energies for the introduction of a subsequent fluoride anion reduces from −43.8 kcal/mol in the

dx.doi.org/10.1021/ic2001706 |*Inorg. Chem.* 2011, 50, 3141–3152

Table 1. Calculated and Experimental Bond Lengths, Å, and Uranyl Vibrational Wavenumbers, cm^{-1}, of the $[UO_2F_n(H_2O)_{5-n}]^{2-n}$ Complexes

	$[UO_2(H_2O)_5]^{2+}$				$[UO_2(H_2O)_5]^{2+}\cdot 5H_2O$				
	gas		aqueous		gas		aqueous		
	B3LYP	BP86 [a]	B3LYP	BP86 [a]	B3LYP	BP86	B3LYP	BP86	expt [b]
U=O	1.748	1.773 (1.772)	1.758	1.783 (1.787)	1.759	1.789 (1.789)	1.768	1.800 (1.797)	1.76
$U-OH_2$	2.499	2.481 (2.494)	2.469	2.458 (2.450)	2.466	2.464 (2.468)	2.428	2.431 (2.439)	2.41
ν_{symm}	927	864 (891)	898	840 (859)	899	843 (867)	878		870
ν_{asymm}	1015	958 (883)	960	911 (922)	991	922 (940)	939		965

	$[UO_2(H_2O)_4F]^{+}$			
	gas		aqueous	
	B3LYP	BP86	B3LYP	BP86
U=O	1.771	1.795 (1.798)	1.776	1.802 (1.807)
$U-OH_2$	2.548	2.539 (2.557)	2.515	2.510 (2.510)
U−F	2.107	2.104 (2.091)	2.146	2.134 (2.128)
ν_{symm}	881	827 (846)	863	808 (825)
ν_{asymm}	962	910 (927)	917	869 (877)

	$[UO_2(H_2O)_3F_2]^0$ structure 1				$[UO_2(H_2O)_3F_2]^0$ structure 2			
	gas		aqueous		gas [c]		aqueous [c]	
	B3LYP	BP86	B3LYP	BP86	B3LYP [3.4]	BP86 [2.5]	B3LYP [1.6]	BP86 [0.02]
U=O	1.785	1.814 (1.813)	1.792	1.820 (1.826)	1.783	1.809 (1.809)	1.792	1.820 (1.825)
$U-OH_2$	2.666	2.657 (2.663)	2.652	2.579 (2.577)	2.594	2.594 (2.605)	2.559	2.562 (2.568)
U−F	2.157	2.150 (2.154)	2.167	2.165 (2.160)	2.180	2.170 (2.210)	2.183	2.170 (2.164)
ν_{symm}	851	798 (824)	831	779 (793)	856	806 (826)	831	779 (793)
ν_{asymm}	928	876 (898)	881	831 (835)	935	886 (905)	879	832 (838)

	$[UO_2(H_2O)_2F_3]^{-}$ structure 1				$[UO_2(H_2O)_2F_3]^{-}$ structure 2				
	gas		aqueous		gas [c]		aqueous [c]		
	B3LYP	BP86	B3LYP	BP86	B3LYP [8.6]	BP86 [9.4]	B3LYP [6.6]	BP86 [6.9]	expt [b]
U=O	1.805	1.841 (1.842)	1.803	1.834 (1.838)	1.799	1.828 (1.828)	1.807	1.832 (1.842)	1.80
$U-OH_2$	2.620, 3.715	2.594, 3.614 (2.605, 3.658)	2.566, 4.172	2.588, 4.033 (2.507, 3.888)	2.776	2.804 (2.790)	2.610	2.625 (2.625)	2.47
U−F	2.192	2.183 (2.183)	2.215	2.196 (2.203)	2.221	2.211 (2.219)	2.221	2.226 (2.203)	2.25
ν_{symm}	812	777 (783)	807	761 (777)	831	814 (822)	805	761 (767)	
ν_{asymm}	884	832 (869)	854	809 (814)	901	850 (853)	848	809 (804)	

	$[UO_2(H_2O)F_4]^{2-}$ structure 1				$[UO_2(H_2O)F_4]^{2-}$ structure 2				
	gas		aqueous		gas [c]		aqueous [c]		
	B3LYP	BP86	B3LYP	BP86	B3LYP [34.7]	BP86 [35.1]	B3LYP [11.0]	BP86 [11.9]	expt [b]
U=O	1.820	1.850	1.819	1.850	1.824	1.856	1.824	1.857 (1.860)	1.80
$U-OH_2$	4.022	4.003	3.958	3.917	2.710	2.701	2.672	2.685 (2.715)	2.48
U−F	2.250	2.240	2.230	2.220	2.260	2.270	2.250	2.244 (2.248)	2.26
ν_{symm}	789	741 (757)	786	737 (755)	776	727	778	726 (740)	
ν_{asymm}	861	815 (830)	825	778 (784)	845	794	814	765 (771)	

	$[UO_2F_5]^{3-}$				$[UO_2F_5]^{3-}\cdot 5H_2O$				
	gas		aqueous		gas		aqueous		
	B3LYP	BP86	B3LYP	BP86	B3LYP	BP86	B3LYP	BP86	expt [b]
U=O	1.842	1.878 (1.876)	1.835	1.871 (1.874)	1.804	1.832 (1.831)	1.811	1.837 (1.840)	1.80
U−F	2.343	2.337 (2.338)	2.300	2.294 (2.281)	2.365	2.361 (2.370)	2.328	2.330 (2.326)	2.26
ν_{symm}	740	688 (694)	757	705 (716)	803	754 (775)	799	751 (764)	784
ν_{asymm}	806	752 (768)	790	739 (745)	865	825 (843)	836	788 (808)	850

[a] The structural properties calculated at the RECP/BP86 level are given, while the ADF/ZORA/BP86/TZP values are given in parentheses. [b] EXAFS data from ref 24. [c] See Figure 2 and the text for structures 1 and 2. The energy differences between structures 1 and 2 are given in square brackets (kcal/mol).

dx.doi.org/10.1021/ic2001706 |*Inorg. Chem.* 2011, 50, 3141–3152

Table 2. Aqueous-Phase Calculated Ligand Binding Energies (BE in kcal/mol), Mayer Bond Orders for the U═O Bond, and Atomic Mulliken Charges on Uranium Atoms in the $UO_2F_n(H_2O)_{5-n}]^{2-n}$ Complexes Obtained at the ADF/ZORA/TZP/BP86/COSMO Level

			Mulliken charges on uranium atoms		U═O Mayer bond orders	
n	calculated ligand BE[b]	experimental successive ligand BE[c]	gas	aqueous	gas	aqueous
0	−95.8		2.364	2.482	2.150	2.065
1	−139.6 (−43.8)	−7.04	2.304	2.418	2.105	2.032
2	−176.2 (−36.6)	−5.00	2.286	2.330	2.060	1.989
2[a]	−176.0 (−36.4)		2.321	2.319	2.060	1.982
3	−205.2 (−29.0)	−2.82	2.215	2.257	1.987	1.935
3[a]	−210.5 (−34.3)		2.260	2.275	2.000	1.960
4	−234.3 (−23.8)	−1.28	2.235	2.241	1.944	1.920
4[a]	−222.9 (−17.8)		2.200	2.154	1.907	1.889
5	−230.6 (+3.70)	1.00	2.094	2.095	1.854	1.844

[a] These are structures 2 for the species with n = 2, 3, and 4, respectively (Figure 2 and text). [b] The ligand BEs are described as $[UO_2]^{2-n} + nF^- + (5 - n)$-$H_2O \rightarrow [UO_2F_n(H_2O)_{5-n}]^{2-n}$. The BEs ($\Delta E$) for successive fluoride ligands are given in parentheses and are calculated as $\Delta E_{\text{successive binding}} = \Delta E_{\text{binding}}{}^{n} - \Delta E_{\text{binding}}{}^{n-1}$, where n is the number of fluoride ligands. [c] Experimental successive ligand BEs were taken from ref 86.

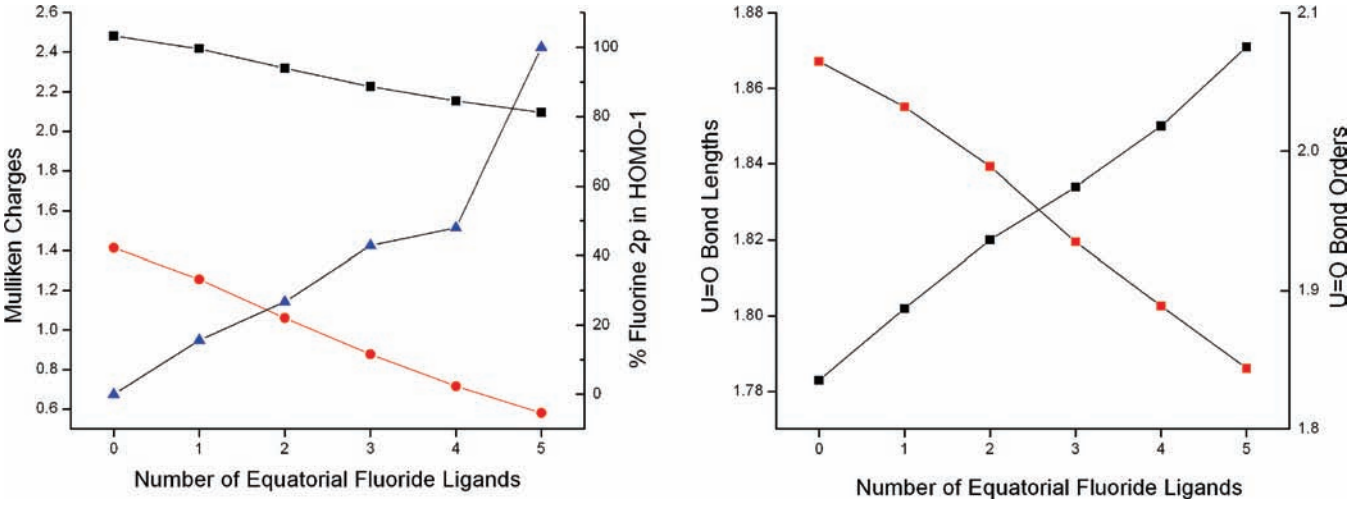

Figure 3. Left: Variation of the Mulliken charges on the uranium atom (black) and uranyl moiety (red) and the F 2p contribution to the HOMO−1 (blue) with an increase in the number of fluoride ligands. Right: Variation of the U═O bond lengths (black) and bond orders (red) with an increase in the number of fluoride ligands. All values were calculated at the ADF/ZORA/BP86/TZP/COSMO level.

case of $[UO_2(H_2O)_5]^{2+}$ to 3.70 kcal/mol in the case of $[UO_2(H_2O)F_4]^{+}$. Further examination of Table 2 reveals that the calculated successive ligand BEs overestimate the experimental values significantly because of the poor performance of the chosen solvation model for calculating ligand BE and activation energies.[12,24,78] The use of extended second and third aquo coordination spheres in addition to the implicit polarizable continuum model around the uranyl complexes would lead to improvements in the calculated ligand BEs.[79]

Electronically, the first few virtual molecular orbitals in all of the uranyl compounds are all of U 5f character (Figure 4A,B). This is generally expected for $5f^0$ uranium(VI) complexes. The highest occupied molecular orbitals (HOMOs) are all uranyl-based and are almost identical in all optimized structures of the $[UO_2F_n(H_2O)_{5-n}]^{2-n}$ compounds. They are of σ character with a 5f atomic contribution from the uranium atom and 2p contributions from the oxygen atoms of the uranyl group (Figure 4C,D). Contributions from the 6p atomic orbitals of uranium are also found in the HOMO σ orbitals for these complexes. However, there are sometimes very minor contributions from the ligand 2p orbitals in π character to the HOMOs in these complexes. The HOMO−1 to HOMO−4 orbitals in all of the complexes are generally π-type orbitals formed from the 2p-type atomic orbitals of the equatorial ligands as well as, in most cases, 2p orbital contributions from the uranyl oxo atoms in a π-bonding scheme. Contributions from the U 6p and 6d orbitals to the HOMO to HOMO−4 orbitals are minor and amount to not more than 1.3% and 2.5%, respectively. The increase in the number of fluoride ligands down the series can be observed in the evolution of the fluorine 2p contributions to the HOMO−1 (Figure 3). There is scant evidence for any form of π competition between the uranyl oxo atoms and the equatorial ligands. A more ionic Lewis base effect appears to be a more plausible explanation for the increase in the U═O and U−F bond lengths with an increase in the number of fluoride ligands in the equatorial plane. In general, the HOMO−1 orbitals are similar in all of the complexes except in $[UO_2F_5]^{3-}$ and $[UO_2(H_2O)_5]^{2+}$, for which there are no contributions to their HOMO−1 orbitals from the uranyl oxo atoms (Figure 4).

dx.doi.org/10.1021/ic2001706 |*Inorg. Chem.* 2011, 50, 3141–3152

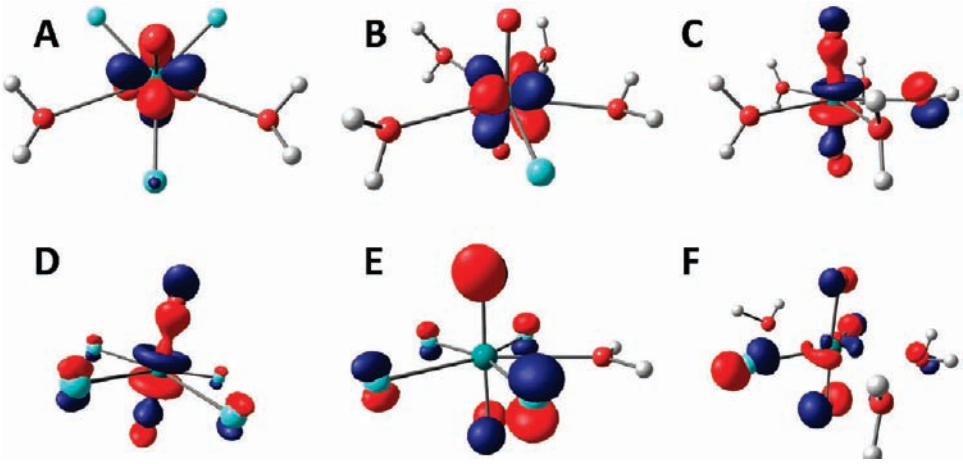

Figure 4. Selected frontier molecular orbitals of $[UO_2F_n(H_2O)_{5-n}]^{2-n}$ member structures optimized at the ADF/ZORA/BP86/TZP/COSMO level: (A) LUMO of $[UO_2(H_2O)_2F_3]^-$ structure 2, (B) LUMO of $[UO_2(H_2O)_4F]^+$, (C) HOMO of $[UO_2(H_2O)_5]^{2+}$, (D) HOMO of $[UO_2F_5]^{3-}$, (E) HOMO−1 of $[UO_2(H_2O)F_4]^{2-}$, and (F) HOMO−1 of $[UO_2(H_2O)_3F_2]^0$ structure 2.

Structurally, the $[UO_2F_5]^{3-}$ complex belongs to the D_{5h} symmetry group in both the gas and aqueous phases (some slight loss in symmetry) in agreement with experimental solution[24] and solid-state[26] observations. Optimization in solution results in a slight contraction of the U−F bonds by approximately 0.04 Å while having little effect on the U═O bonds. The calculated symmetric and asymmetric stretching vibrational frequencies of the uranyl group of $[UO_2F_5]^{3-}$ deviate significantly from the experimental values.[80,81] The discrepancy is most likely due to the insufficient description of the aqueous environment around the ionic complex by the implicit COSMO used. Indeed, better agreement was obtained after the inclusion of five water molecules in the second coordination sphere around the uranyl group (Table 1). The presence of a second coordination sphere with five water molecules results in the shortening of the U═O bond by 0.02−0.04 Å while causing an increase in the U−F bonds lengths.

The $U-OH_2$ bonds of the optimized C1 structure of $[UO_2(H_2O)_5]^{2+}$ are generally of two types in aqueous solution: four water ligands arranged orthogonally to the equatorial plane and the last aquo ligand almost parallel to the equatorial plane. This orientation is only slightly more stable than the symmetrical D_5 and D_{5h} structures. Electronically, the introduction of D_5 and D_{5h} high symmetries alters the orbital ordering in the complex. The major effect of imposing the D_5 and D_{5h} symmetries is a stabilization of the σ-type HOMO in the C1 structure relative to the π-type HOMO−1. The calculated U═O and $U-OH_2$ bond lengths in the minimum structure are in good agreement with both the experimental results and previous theoretical calculations.[76,82] Although the O═U═O bond angles in this molecule are slightly bent by 0.12−4.04°, it should be noted that Perron et al. have mentioned that the XANES data of $[UO_2(H_2O)_5]^{2+}$ could actually be explained with O═U═O bond angles of not less than 160°.[83] Similar to $[UO_2F_5]^{3-}$ (Table 1), the addition of five water molecules in the second coordination sphere results in better agreement between the calculated and experimental uranyl stretching vibrational frequencies.

The addition of a second coordination sphere containing five water molecules to the structures of $[UO_2(H_2O)_5]^{2+}$ and $[UO_2F_5]^{3-}$ not only results in greater agreement between the experimental and calculated vibrational frequencies but also allows the experimental range of the U═O bond lengths in the $[UO_2F_n(H_2O)_{5-n}]^{2-n}$ complexes to be accurately captured by the theoretical calculations (Table 1). The difference in the experimental U═O bond lengths of $[UO_2(H_2O)_5]^{2+}$ and $[UO_2F_5]^{3-}$ is 0.04 Å, in contrast to 0.08−0.09 Å obtained using COSMO but in full agreement with 0.037−0.043 Å using a combination of the COSMO model with five water molecules in the second coordination sphere. This is particularly important given that recent experimental work has revealed little evidence for variation in the U═O bond lengths among the species in the $[UO_2F_n(H_2O)_{5-n}]^{2-n}$ series.[24]

The structure of the $[UO_2(H_2O)_4F]^+$ complex (Figure 2H) is a simple arrangement of the oxygen atoms of the four water ligands and the fluoride ion in the equatorial plane. The uranyl O═U═O angle in this complex ranges from 168.8° to 174.4° in the gas and aqueous phases. A comparison to $[UO_2(H_2O)_5]^{2+}$ indicates a slight increase in the U═O (0.02 Å) and $U-OH_2$ (0.045 Å) bond lengths accompanied by a corresponding decrease in the vibrational wavenumbers of the U═O bond stretch. This increase in the U═O bond lengths (and also in the U−F bond lengths down the series) is directly related to the decrease in the calculated charges on the uranium atom and the uranyl group (Figure 3). The electron-donating fluoride ligand leads to a decrease in the charge on the actinide center, resulting in weaker U−F bonds as more fluoride ligands are added with an added effect of some electrostatic repulsion with the uranyl oxo atoms and equatorial water ligands.[13]

There are many possible arrangements of the fluoro and aquo ligands in the complexes intermediate between $[UO_2(H_2O)_4F]^+$ and $[UO_2(H_2O)F_4]^{2-}$. For $[UO_2(H_2O)_3F_2]^0$, only the structures in which all of the aquo and fluoro ligands lie in the equatorial region were considered. Structure 1 (or the cis structure with neighboring fluoro ligands; Figure 2F) was calculated to be approximately 3.4 and 1.6 kcal/mol less stable than structure 2 (or the trans structure with nonneighboring fluoro ligands; Figure 2G) at the B3LYP/6-311++G** level in the gas and aqueous phases, respectively. The energy differences between these structural isomers are, however, 0.02 and 0.12 kcal/mol at the RECP-BP86 and ZORA-BP86 levels, respectively, in aqueous solution. The small magnitude of this energy difference might suggest coexistence or facile interconvertibility. In addition, the calculated geometrical parameters and vibrational frequencies for both structures are identical especially in

dx.doi.org/10.1021/ic2001706 |*Inorg. Chem.* 2011, 50, 3141–3152

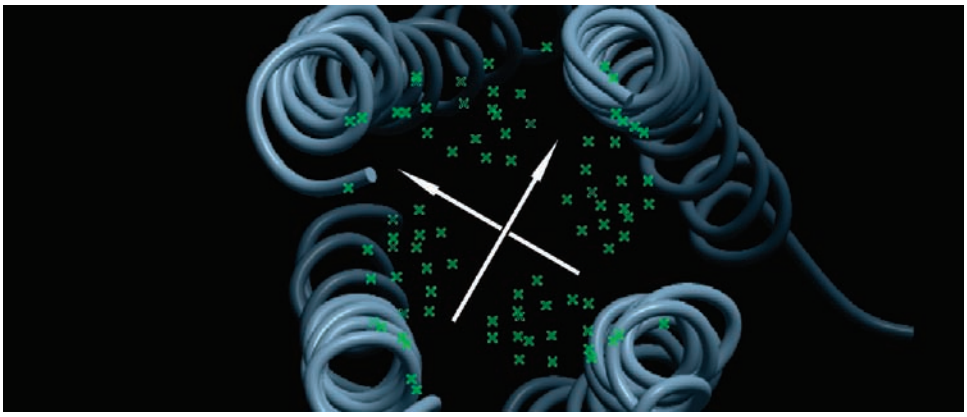

Figure 5. Atoms of the isoleucine residues (represented as green crosses) at the N-terminal end of cavity 2. The protruding side chains form a crosslike space into which the uranyl group and equatorial fluoride ligands of $[UO_2F_5]^{3-}$ are embedded. The two white arrows depict the two possible alignments of the uranyl moiety and the equatorial ligands.

the aqueous phase. The only exception to this is a U−OH_2 bond in structure 1, which was calculated to be about 0.22 Å longer than all of the U−OH_2 bonds in structure 2.

The structure corresponding to the alignment of three neighboring fluoro ligands as well as one aquo ligand in the equatorial plane represents the most stable conformation of the $[UO_2(H_2O)_2F_3]^-$ complex (structure 1, Figure 2D). The other aquo ligand is at a long distance of 3.57−4.17 Å from the uranium atom. This long distance representing an aquo ligand outside the first coordination sphere was, however, not observed experimentally.[24] Structure 1 was calculated to be approximately 6.6−9.4 kcal/mol more stable than the structure corresponding to two nonneighboring aquo ligands with the fluoro ligands aligned in a triangular fashion at the equatorial plane (structure 2, Figure 2E). The calculated U═O and U−F bond lengths for structure 2 are in good agreement with experimental data in contrast to the U−OH_2 bonds, which were calculated to be 0.14−0.16 Å longer than was experimentally observed.[24] It might be that the addition of counterions further stabilizes structure 2 enough to reach quantitative agreement with experimental observation.[11]

Computed local minimum structures for the $[UO_2(H_2O)F_4]^{2-}$ complex have generally been structures with the water ligand at about 3.90−4.02 Å away from the uranium atom[12] (structure 1, Figure 2B). However, experimental studies in crystal structures or solution have indicated the presence of a short U−OH_2 bond of about 2.48 or 2.11 Å in length, respectively.[24,81] The C_{2v} structure (structure 2, Figure 2C) corresponding to this arrangement has two imaginary frequencies in both gas- and continuum-phase DFT calculations. Structure 2 was calculated to convert to structure 1 or to dissociate to $[UO_2F_4]^{2-}$ and an outgoing water molecule with conversion or dissociation energies of 10−13 and 5.4−6.3 kcal/mol, respectively, in aqueous solution (Table 1). Carr−Parrinello molecular dynamics simulations by Bühl et al.[11] have been used to show that the addition of two ammonium counterions stabilizes the "experimental" geometry of structure 2 by about 2−4 kcal/mol, thus possibly justifying the experimental observation.[24,81] It would, therefore, appear that the inclusion of counterions according to Bühl et al. in calculations on the $[UO_2(H_2O)F_4]^{2-}$ complex is essential.[11]

$[UO_2F_5]^{3-}$ Docked in the Cavities of the RHCC. The terminal cavities (N and C terminals or cavities 1 and 4, respectively) of the RHCC protein are lined at the N- and C-terminal ends by isoleucine residues. The intermediate cavities 2 and 3 are, however, bounded at their N- and C-terminal ends by isoleucine and leucine residues, respectively (Figure 1). These hydrophobic residues are oriented such that their side chains protrude into the axial channel of the protein (Figures 1 and 5). Eight residues from each monomer unit, which are amino acids less hydrophobic than leucine and isoleucine, form a ring around each cavity.[5] The cavities range in size from 140 to 280 $Å^3$ in the native protein and are occupied by water clusters. In this work, $[UO_2F_5]^{3-}$ and cisplatin were docked in these cavities and optimized using QM/MM. Only preliminary docking simulations were carried out for $[Pt(CN)_6]^{2-}$. $[UO_2F_5]^{3-}$ was used as a representative for the $[UO_2F_n(H_2O)_{5-n}]^{2-n}$ complexes because of the rigidity of the bonds between the uranyl group and the equatorial ligands and the resulting relative ease to dock in the hydrophobic cavities. This is in spite of the fact that $[UO_2F_5]^{3-}$ is formed only at high fluoride concentrations.[24] $[UO_2F_5]^{3-}$ can be thought of as a model system with the protein environment having similar structural and electronic effects on the other members of the pentaaquofluoro series.

An infinite number of possible orientations of the uranyl group can be expected if $[UO_2F_5]^{3-}$ is embedded in a chemically uniform and spherical hydrophobic cavity. However, docking of this complex in all of the RHCC cavities indicates the presence of two favored orientations of the uranyl group with respect to the axial channel. The uranyl group can only be oriented along the two axes perpendicular to the RHCC axis in all of the hydrophobic cavities (Table 3). The equatorial fluoro ligands occupy the second axis orthogonal to the axial channel, and no possible alignment of the O═U═O group along the RHCC axial channel was found.

The presence of these minima orientations of the embedded complex along axes orthogonal to the axial channel can be explained by two observations. First, the cavities of the RHCC protein are chemically heterogeneous and roughly cylindrical with isoleucine and/or leucine residues (ah layer) pointing into the center of the helix, while the backbone of the arginine and tyrosine residues (de layer) form a ring bounding the cavity.[5,10] The uranyl complex embedded in the cavities is always positioned closest to the isoleucine residues at the N-terminal end of the cavities, except in cavity 4, the C-terminal cavity, in which the complex is positioned nearest to the residues at the C-terminal end because of exposure to the aqueous environment. Maximum

dx.doi.org/10.1021/ic2001706 |*Inorg. Chem.* 2011, 50, 3141–3152

Table 3. Calculated Relative Energies (kcal/mol), Frontier Gaps (eV), and Structural Features of the Two Orientations of the $[UO_2F_5]^{3-}$ Complex in the Hydrophobic Cavities of Tetrabrachion

cavity	alignment[a]	$\Delta\Delta G_{docking}$[b]	$\Delta\Delta G_{QM/MM}$	frontier gap (eV)	$R_{U=O}$ (Å)	R_{U-F} (Å)	$\angle_{O=U=O}$ (deg)
1	a			2.709	1.877−1.892	2.272−2.372	177.2
	b	0.00	10.12	2.634	1.874−1.877	2.273−2.420	176.8
2	a			2.677	1.865−1.876	2.321−2.348	179.2
	b	0.03	0.05	2.702	1.878−1.894	2.324−2.355	178.9
3	a			2.489	1.864−1.887	2.266−2.391	175.8
	b	0.03	5.77	2.366	1.860−1.892	2.260−2.405	172.1
4	a			2.794	1.877−1.909	2.268−2.391	177.9
	b	0.01	8.33	2.793	1.854−1.866	2.214−2.365	177.5
gas				2.694	1.878	2.337	180.0
aqueous				2.728	1.871	2.294	180.0

[a] The two alignments of $[UO_2F_5]^{3-}$ in the cavities are labeled a and b according to their relative energies. [b] The free energies, $\Delta\Delta G$, are given as the difference $\Delta G_A - \Delta G_B$.

separation from the leucine residues at the C-terminal end of the cavities could be explained based on steric considerations. The leucine residues simply penetrate deeper into the axial channel, affording lesser space for the embedded ligand. On the other hand, the isoleucine side chains at the N-terminal ends of the cavities are more "open" and have greater access into the axial channel (Figure 1) and the aqueous environment in the case of cavity 1, the N-terminal cavity.

Second, the side chains of the isoleucine residues pointing into the axial channel from each monomer backbone form a crosslike space bounded at the four edges by the protein backbone (Figure 5). It is near this crosslike opening in the isoleucine residues partitioning the axial channel that the two possible arrangements of the uranyl moiety and the five equatorial fluoride ligands of the $[UO_2F_5]^{3-}$ complex fit. Typical distances between the alkyl hydrogen atoms of the isoleucine residues and the atoms of the $[UO_2F_5]^{3-}$ complex ranged from 2.0 to 4.8 Å after the docking.

QM/MM Calculations on $[UO_2F_5]^{3-}$ Embedded in the RHCC Cavities. Structurally, the D_{5h} symmetry of the $[UO_2F_5]^{3-}$ complex is lifted and five different U−F bond lengths were observed after QM/MM optimization in all of the cavities. For each cavity, the orientation with longer U−F bonds or shorter distances between its fluoro ligand and the hydrogen atoms of the isoleucine residues is less favorable energetically (Table 3). Electronically, there is some correspondence between the U−F bond lengths and the calculated HOMO−LUMO gaps of the embedded ligands. After considering energy constraints and the calculated structural parameters, it can be concluded that there is a possibility of experimentally observing the two ligand orientations in only cavity 2.

The maximum energy difference between the two orientations in the four cavities obtained using the docking procedure, $\Delta\Delta G_{docking}$, is 0.03 kcal/mol (Table 3). The orientations are, therefore, essentially isoenergetic and the magnitude of this energy barrier suggests that both orientations should be experimentally observed in all of the cavities with a high probability of interconversion. However, the calculated energy barriers,[84] $\Delta\Delta G_{QM/MM}$ (Table 3), indicate that the two orientations of the embedded QM/MM-optimized $[UO_2F_5]^{3-}$ complex should be observable only in cavity 2, the largest cavity. Only in this cavity are they still isoenergetic, even at the QM/MM level. There is strong experimental evidence for the existence of the two orientations of uranyl fluoride in this cavity, as found by the calculations.[53] The other cavities all have one high-energy conformation, resulting in a low probability of experimental observation.

The calculation of the free energies associated with the replacement of the water clusters in the native RHCC cavities by the $[UO_2F_5]^{3-}$ ligand is difficult and requires averaging over the configuration space of the protein−ligand system. This is particularly important because the water clusters move on much faster time scales than the uranyl complex. Using a few snapshots of the protein−ligand system in calculating the free energies associated with displacement of the native water clusters by $[UO_2F_5]^{3-}$ may, therefore, be misleading. However, intuitively, the exchange of the water clusters with uranyl fluorides would be expected to be exergonic.[4,5] The free energy associated with displacement of the water clusters could be expected to be dominated by a large entropic contribution[6] even though the enthalpy contribution is expected to be slightly positive because of transfer of the uranyl complex from the aqueous medium into a cavity surrounded by hydrophobic residues.

Both orientations in cavity 1, the N-terminal cavity, have U═O and U−F bond lengths within 0.02 and 0.08 Å of the gas-phase structural parameters, respectively (Table 3). An examination of the electronic structure of the embedded ligands reveals a reduction of the HOMO−LUMO gap by approximately 0.06 eV in the less energetically favored orientation. This orientation also has the larger U−F bond deformation and a greater change in the O═U═O bond angle.

The structural parameters of the embedded ligands in cavity 2 (the largest cavity) are essentially identical with those calculated for the gas-phase structure. The U═O and U−F bond lengths are all within 0.03 Å of the calculated gas-phase values. In addition, the uranyl bond angles are within 1.2° of the gas-phase structures. The similarity of the ligands embedded in this cavity to the gas-phase complex is also reflected in the calculated uranyl stretching vibrational frequencies. Electronically, the HOMO−LUMO gaps and the description of the frontier orbitals for the ligand embedded in this cavity are similar (to within about 0.02 eV) to those calculated for the gas-phase structure. The similarity of both uranyl conformations to the gas-phase structure is most likely due to the size of the cavity, with a large size of the cavity allowing for minimal interaction with the hydrogen atoms of the isoleucine residues.

The effects of the RHCC framework on the geometries of the embedded ligands are more pronounced in cavity 3 than in the

dx.doi.org/10.1021/ic2001706 |Inorg. Chem. 2011, 50, 3141–3152

Table 4. Computed Structural Parameters of Cisplatin

	gaseous		solution			BP86	
parameter	B3LYP	BP86	B3LYP	BP86	expt[a]	structure 1	structure 2
Pt−Cl	2.310	2.303	2.349	2.336	2.330	2.312	2.314
Pt−N	2.104	2.092	2.079	2.068	2.010	2.099	2.101
N−Pt−N	98.19	99.27	92.22	92.99	87.0	98.81	98.26
Cl−Pt−Cl	95.54	95.78	93.92	94.10	91.9	95.53	95.63

[a] Crystal structure from ref 82.

first two cavities. Deviations of the U═O and U−F bond lengths by 0.03 and 0.07 Å, respectively, from the gas-phase values were calculated in cavity 3. The uranyl bond angle was decreased by 4.2 and 7.9° in the two possible orientations in this cavity. A significant decrease in the HOMO−LUMO gap by 0.21−0.33 eV was calculated in the ligands embedded in this cavity compared to the gas-phase complex.

The less energetically favorable orientation in cavity 4, the C-terminal cavity, has significant deformation of the U−F bonds by up to 0.12 Å. There is lesser deformation of the U−F bonds (0.02−0.07 Å) and longer U═O bonds in the more energetically accessible orientation (Table 3). The U═O bonds in both orientations are, however, within 0.03 Å of the gas-phase structure. In addition, the HOMO−LUMO gaps for both orientations of the ligand are similar and are about 0.1 eV larger than the gas-phase value.

Other Ligands Embedded in the RHCC. Because of the potential use of the cavities of this coiled-coil protein as a delivery vehicle for therapeutic molecules, we have also explored enclosure of a cisplatin molecule in cavity 2 of the RHCC. Unlike in the case of $[UO_2F_5]^{3-}$, docking and subsequent QM/MM calculations of cisplatin in this cavity indicate that there are more than two possible orientations with respect to the axial channel. Also, there is no preference for alignment or location toward the isoleucine residues at the N-terminal end of the cavity unlike the uranyl complex.

An explanation for this is the absence of a strong oxo axial group that can preferentially anchor toward the isoleucine residues at the N-terminal end of the cavity. The chloro and ammine ligands of cisplatin can, therefore, be oriented in a fairly large number of possible orientations with respect to the RHCC axis. The chemical nature of the ammine ligands also allows for interaction with the carbonyl groups of the cavity wall. On the other hand, preliminary docking of the hexacyanoplatinate complex, $[Pt(CN)_6]^{2-}$, in the largest cavity revealed only two orientations reminiscent of those observed for the uranyl complex. The presence of two favored orientations for $[UO_2F_5]^{3-}$ and $[Pt(CN)_6]^{2-}$ in the protein cavities suggests that these alignments will exist for molecules with strong axial groups in an octahedral- or pentagonal-bipyramidal framework.

The calculated structural parameters for two randomly selected poses of cisplatin embedded in the largest cavity of the RHCC protein are compared to the calculated gas- and aqueous-phase structures as well as the experimental crystal structure[85] in Table 4. The optimized structures of these two poses are essentially similar to the gas-phase structure even though there is a minute elongation of the Pt−Cl bond as well as contraction of the N−Pt−N bond angle. This is largely not surprising because very few water molecules actually penetrate the axial channel of the RHCC protein and cavity 2 is large enough to allow the molecule to exist in a "pseudogaseous" state.

CONCLUSIONS

A systematic study of pentacoordinated aquo and fluoro uranyl complexes has been carried out using two different relativistic methods, the RECPs and ZORA with all-electron basis set, in conjunction with the B3LYP and BP86 density functionals. The effects of an aqueous medium on the geometrical structure, ligand BEs, and the electronic structure were investigated using COSMO as well as an explicit second coordination sphere. The conformational alignments, electronic structures, and geometrical parameters of $[UO_2F_5]^{3-}$ and cisplatin embedded in the hydrophobic cavities of the tetrabrachion coiled coil have been determined with the hybrid QM/MM approach. The studies of cisplatin and $[UO_2F_5]^{3-}$ inside the hydrophobic cavities were motivated by the need for insight into therapeutic usage of the protein in drug delivery and structural or conformational alignment reasons, respectively.

The inclusion of solvation effects using COSMO generally leads to only slight increases in the U═O bonds lengths, in contrast to a contraction of the U−F bonds. This effect is associated with decreases in the uranyl stretching vibrational frequencies. The calculated U═O bond lengths increase as the number of fluoride ligands are increased in both the gas and aqueous phases. The range of the U═O bond lengths from $[UO_2(H_2O)_5]^{2+}$ to $[UO_2F_5]^{3-}$ is, however, only accurately captured after the inclusion of five water molecules in the second coordination sphere. The inclusion of water molecules in the second coordination sphere also results in better agreement between the calculated and experimental uranyl vibrational frequencies.

Although the docking procedure used in this contribution indicates the presence of two favored orientations of the $[UO_2F_5]^{3-}$ complex in all four hydrophobic cavities of the tetrabrachion coiled-coil protein, the calculated relative free energies of embedded complexes optimized at the QM/MM level, however, reveal that both orientations can only be experimentally observed in cavity 2, the largest cavity. There is strong experimental evidence for these orientations, as found by the calculations.[53] In the other three cavities, only one conformation is energetically accessible. The two possible orientations of the uranyl complexes in the protein cavities are along the two axes perpendicular to the protein channel axis. There is no possible orientation of the embedded ligands along the channel axis. The uranyl pentafluoride is generally associated with the isoleucine residues at the N-terminal end of the protein cavities. This is due to a combination of steric effects and interaction with the alkyl side chains of the isoleucine residues. The presence of two ordered orientations of the uranyl complexes in the hydrophobic cavities is not unique. Docking of the hexacoordinated $[Pt(CN)_6]^{2-}$ complex also reveals a similar structure in cavity 2 of the protein. On the other hand, the anticancer drug cisplatin shows no preferred orientations in the protein cavities.

In general, there is little change in the U═O bond lengths upon embedding of the complexes, with a maximum change of 0.03 Å from the gas-phase value of 1.878 Å at the BP86/RECP level. The largest structural changes are seen in the U−F bond lengths and O═U═O bond angles. An examination of the structural features, HOMO−LUMO gaps, and uranyl stretching

dx.doi.org/10.1021/ic2001706 |Inorg. Chem. 2011, 50, 3141–3152

vibrational frequencies of the uranyl complexes embedded in cavity 2 reveals great similarity to the gas-phase structure.

■ ASSOCIATED CONTENT

Supporting Information. Graphical representations of the $[UO_2F_5]\cdot 5H_2O^{3-}$ and $[UO_2(H_2O)_5]\cdot 5H_2O^{2+}$ complexes optimized at the ADF/ZORA/BP86/TZP/COSMO level and a sample ADT input file. This material is available free of charge via the Internet at http://pubs.acs.org.

■ AUTHOR INFORMATION

Corresponding Author
*E-mail: schrecke@cc.umanitoba.ca.

■ ACKNOWLEDGMENT

S.O.O. thanks the Provincial Government of Manitoba, Canada, for partial funding for this project via the Manitoba Graduate Scholarship. G.S. and J.S. acknowledge financial support from the Natural Sciences and Engineering Research Council of Canada. The Bugaboo cluster of the Western Canada Research Grid (WestGrid) and the PNL/EMSL Chinook supercomputer were used for all of the computations in this work.

■ REFERENCES

(1) Burkhard, P.; Stetefeld, J.; Strelkov, S. V. *Trends Cell Biol.* **2001**, *11*, 82.
(2) Eriksson, M.; Hassan, S.; Larsson, R.; Linder, S.; Ramqvist, T.; Lovborg, H.; Vikinge, T.; Figgemeier, E.; Muller, J.; Stetefeld, J.; Dalianis, T.; Ozbek, S. *Anticancer Res.* **2009**, *29*, 11.
(3) http://www.pdb.org/pdb/explore/explore.do?structureId=1FE6.
(4) Ozbek, S.; Muller, J. F.; Figgemeier, E.; Stetefeld, J. *Acta Crystallogr., Sect. D* **2005**, *61*, 477.
(5) Stetefeld, J.; Jenny, M.; Schulthess, T.; Landwehr, R.; Engel, J.; Kammerer, R. A. *Nat. Struct. Biol.* **2000**, *7*, 772.
(6) Vaitheeswaran, S.; Yin, H.; Rasaiah, J. C.; Hummer, G. *Proc. Natl. Acad. Sci. U.S.A.* **2004**, *101*, 17002.
(7) Yin, H.; Hummer, G.; Rasaiah, J. C. *J. Am. Chem. Soc.* **2007**, *129*, 7369.
(8) McFarlane, A. A.; Orriss, G. L.; Stetefeld, J. *Eur. J. Pharmacol.* **2009**, *625*, 101.
(9) Ozbek, S.; Muller, J. F.; Figgemeier, E.; Stetefeld, J. *Acta Crystallogr., Sect. D* **2005**, *61*, 477.
(10) Stetefeld, J.; Jenny, M.; Schulthess, T.; Landwehr, R.; Engel, J.; Kammerer, R. A. *Nat. Struct. Biol.* **2000**, *7*, 772.
(11) Bühl, M.; Schreckenbach, G.; Sieffert, N.; Wipff, G. *Inorg. Chem.* **2009**, *48*, 9977.
(12) Bühl, M.; Sieffert, N.; Wipff, G. *Chem. Phys. Lett.* **2009**, *467*, 287.
(13) Gaillard, C.; El Azzi, A.; Billard, I.; Bolvin, H.; Hennig, C. *Inorg. Chem.* **2005**, *44*, 852.
(14) Garcia-Hernandez, M.; Willnauer, C.; Krüger, S.; Moskaleva, L. V.; Rösch, N. *Inorg. Chem.* **2006**, *45*, 1356.
(15) Infante, I.; Van Stralen, B.; Visscher, L. *J. Comput. Chem.* **2006**, *27*, 1156.
(16) Infante, I.; Visscher, L. *J. Comput. Chem.* **2004**, *25*, 386.
(17) Macak, P.; Tsushima, S.; Wahlgren, U.; Grenthe, I. *Dalton Trans.* **2006**, 3638.
(18) Paez-Hernandez, D.; Ramirez-Tagle, R.; Codorniu-Hernandez, E.; Montero-Cabrera, L. A.; Arratia-Perez, R. *Polyhedron* **2010**, *29*, 975.
(19) Schreckenbach, G. *Inorg. Chem.* **2002**, *41*, 6560.
(20) Schreckenbach, G.; Hay, P. J.; Martin, R. L. *J. Comput. Chem.* **1999**, *20*, 70.
(21) Shamov, G. A.; Schreckenbach, G.; Vo, T. N. *Chem.—Eur. J.* **2007**, *13*, 4932.
(22) Straka, M.; Dyall, K. G.; Pyykkö, P. *Theor. Chem. Acc.* **2001**, *106*, 393.
(23) Straka, M.; Kaupp, M. *Chem. Phys.* **2005**, *311*, 45.
(24) Vallet, V.; Wahlgren, U.; Schimmelpfennig, B.; Moll, H.; Szabo, Z.; Grenthe, I. *Inorg. Chem.* **2001**, *40*, 3516.
(25) Wang, Q.; Pitzer, R. M. *J. Phys. Chem. A* **2001**, *105*, 8370.
(26) Zachariasen, W. H. *Acta Crystallogr.* **1954**, *7*, 783.
(27) Cramer, C. J. *Essentials of Computational Chemistry: Theories and Models*, 2nd ed.; John Wiley & Sons Ltd.: West Sussex, U.K., 2004; p 17.
(28) Eichinger, M.; Tavan, P.; Hutter, J.; Parrinello, M. *J. Chem. Phys.* **1999**, *110*, 10452.
(29) Field, M. J. *J. Comput. Chem.* **2002**, *23*, 48.
(30) Friesner, R. A.; Guallar, V. *Annu. Rev. Phys. Chem.* **2005**, *56*, 389.
(31) Hu, H.; Elstner, M.; Hermans, J. *Proteins* **2003**, *50*, 451.
(32) Lin, H.; Truhlar, D. G. *Theor. Chem. Acc.* **2007**, *117*, 185.
(33) Murphy, R. B.; Philipp, D. M.; Friesner, R. A. *J. Comput. Chem.* **2000**, *21*, 1442.
(34) Schoneboom, J. C.; Lin, H.; Reuter, N.; Thiel, W.; Cohen, S.; Ogliaro, F.; Shaik, S. *J. Am. Chem. Soc.* **2002**, *124*, 8142.
(35) Senn, H. M.; Thiel, W. *Atomistic Approaches in Modern Biology: From Quantum Chemistry to Molecular Simulations*; Springer−Verlag: Berlin, 2007; Vol. 268, p 173.
(36) Sherwood, P.; de Vries, A. H.; Guest, M. F.; Schreckenbach, G.; Catlow, C. R. A.; French, S. A.; Sokol, A. A.; Bromley, S. T.; Thiel, W.; Turner, A. J.; Billeter, S.; Terstegen, F.; Thiel, S.; Kendrick, J.; Rogers, S. C.; Casci, J.; Watson, M.; King, F.; Karlsen, E.; Sjovoll, M.; Fahmi, A.; Schafer, A.; Lennartz, C. *J. Mol. Struct. THEOCHEM* **2003**, *632*, 1.
(37) Vreven, T.; Morokuma, K.; Farkas, O.; Schlegel, H. B.; Frisch, M. J. *J. Comput. Chem.* **2003**, *24*, 760.
(38) Warshel, A. *Annu. Rev. Biophys. Biomol. Struct.* **2003**, *32*, 425.
(39) Woo, T. K.; Cavallo, L.; Ziegler, T. *Theor. Chem. Acc.* **1998**, *100*, 307.
(40) Warshel, A.; Levitt, M. *J. Mol. Biol.* **1976**, *103*, 227.
(41) Singh, U. C.; Kollman, P. A. *J. Comput. Chem.* **1986**, *7*, 718.
(42) Valiev, M.; Yang, J.; Adams, J. A.; Taylor, S. S.; Weare, J. H. *J. Phys. Chem. B* **2007**, *111*, 13455.
(43) Friesner, R. A.; Guallar, V. *Annu. Rev. Phys. Chem.* **2005**, *56*, 389.
(44) Sauer, J.; Sierka, M. *J. Comput. Chem.* **2000**, *21*, 1470.
(45) Senn, H. M.; Thiel, W. *Angew. Chem., Int. Ed.* **2009**, *48*, 1198.
(46) Shurki, A.; Warshel, A. *Protein Simul.* **2003**, *66*, 249.
(47) Infante, I.; Van Stralen, B.; Visscher, L. *J. Comput. Chem.* **2006**, *27*, 1156.
(48) Infante, I.; Visscher, L. *J. Comput. Chem.* **2004**, *25*, 386.
(49) Faas, S.; Snijders, J. G.; van Lenthe, J. H.; van Lenthe, E.; Baerends, E. J. *Chem. Phys. Lett.* **1995**, *246*, 632.
(50) van Lenthe, E. *J. Comput. Chem.* **1999**, *20*, 51.
(51) van Lenthe, E.; Baerends, E. J.; Snijders, J. G. *J. Chem. Phys.* **1993**, *99*, 4597.
(52) Cornell, W. D.; Cieplak, P.; Bayly, C. I.; Gould, I. R.; Merz, K. M.; Ferguson, D. M.; Spellmeyer, D. C.; Fox, T.; Caldwell, J. W.; Kollman, P. A. *J. Am. Chem. Soc.* **1995**, *117*, 5179.
(53) Stetefeld, J.; Meier, M. Unpublished results.
(54) Stephens, P. J.; Devlin, F. J.; Chabalowski, C. F.; Frisch, M. J. *J. Phys. Chem.* **1994**, *98*, 11623.
(55) Becke, A. D. *J. Chem. Phys.* **1993**, *98*, 5648.
(56) Lee, C. T.; Yang, W. T.; Parr, R. G. *Phys. Rev. B* **1988**, *37*, 785.
(57) Becke, A. D. *Phys. Rev. A* **1988**, *38*, 3098.
(58) Perdew, J. P. *Phys. Rev. B* **1986**, *33*, 8822.
(59) Küchle, W.; Dolg, M.; Stoll, H.; Preuss, H. *J. Chem. Phys.* **1994**, *100*, 7535.
(60) Cao, X. Y.; Moritz, A.; Dolg, M. *Chem. Phys.* **2008**, *343*, 250.
(61) http://www.theochem.uni-stuttgart.de/pseudopotentials/clickpse.en.html.
(62) Bylaska, E. J. d. J. W. A.; Govind, N.; Kowalski, K.; Straatsma, T. P.; Valiev, M.; Wang, D.; Apra, E.; Windus, T. L.; Hammond, J.;

Nichols, P.; Hirata, S.; Hackler, M. T.; Zhao, Y.; Fan, P.-D.; Harrison, R. J.; Dupuis, M.; Smith, D. M. A.; Nieplocha, J.; Tipparaju, V.; Krishnan, M.; Wu, Q.; Van Voorhis, T.; Auer, A. A.; Nooijen, M.; Brown, E.; Cisneros, G.; Fann, G. I.; Fruchtl, H.; Garza, J.; Hirao, K.; Kendall, R.; Nichols, J. A.; Tsemekhman, K.; Wolinski, K.; Anchell, J.; Bernholdt, D.; Borowski, P.; Clark, T.; Clerc, D.; Dachsel, H.; Deegan, M.; Dyall, K.; Elwood, D.; Glendening, E.; Gutowski, M.; Hess, A.; Jaffe, J.; Johnson, B.; Ju, J.; Kobayashi, R.; Kutteh, R.; Lin, Z.; Littlefield, R.; Long, X.; Meng, B.; Nakajima, T.; Niu, S.; Pollack, L.; Rosing, M.; Sandrone, G.; Stave, M.; Taylor, H.; Thomas, G.; van Lenthe, J.; Wong, A.; Zhang, Z. *NWChem, A Computational Chemistry Package for Parallel Computers*, version 5.1; Pacific Northwest National Laboratory: Richland, WA, 2007.

(63) Valiev, V.; Bylaska, E. J.; Govind, N.; Kowalski, K.; Straatsma, T. P.; van Dam, H. J. J.; Wang, D.; Nieplocha, J.; Apra, E.; Windus, T. L.; de Jong, W. A. *Comput. Phys. Commun.* **2010**, *181*, 1477.

(64) Klamt, A. *J. Phys. Chem.* **1995**, *99*, 2224.

(65) Klamt, A.; Schuurmann, G. *J. Chem. Soc., Perkin Trans.* **1993**, *2*, 799.

(66) te Velde, G.; Bickelhaupt, F. M.; van Gisbergen, S. J. A.; Fonseca Guerra, C.; Baerends, E. J.; Snijders, J. G.; Ziegler, T. *J. Comput. Chem.* **2001**, *22*, 931.

(67) Fonseca Guerra, C.; Snijders, J. G.; te Velde, G.; Baerends, E. J. *Theor. Chem. Acc.* **1998**, *99*, 391.

(68) *ADF2009.1*. Theoretical Chemistry, Vrije Universiteit: Amsterdam, The Netherlands, http://www.scm.com.

(69) Swart, M.; van Duijnen, P. T.; Snijders, J. G. *J. Comput. Chem.* **2001**, *22*, 79.

(70) Pye, C. C.; Ziegler, T. *Theor. Chem. Acc.* **1999**, *101*, 396.

(71) Schreckenbach, G.; Shamov, G. A. *Acc. Chem. Res.* **2010**, *43*, 19.

(72) Goodsell, D. S.; Morris, G. M.; Olson, A. J. *J. Mol. Recognit.* **1996**, *9*, 1.

(73) Guilbaud, P.; Wipff, G. *THEOCHEM* **1996**, *366*, 55.

(74) Spiegel, K.; Rothlisberger, U.; Carloni, P. *J. Phys. Chem. B* **2004**, *108*, 2699.

(75) Odoh, S. O.; Schreckenbach, G. *J. Phys. Chem. A* **2010**, *114*, 1957.

(76) Shamov, G. A.; Schreckenbach, G. *J. Phys. Chem. A* **2005**, *109*, 10961; Correction Note. *J. Phys. Chem. A* 2006, *110*, 12072.

(77) Schultz, N. E.; Zhao, Y.; Truhlar, D. G. *J. Phys. Chem. A* **2005**, *109*, 4388.

(78) Vallet, V.; Wahlgren, U.; Szabo, Z.; Grenthe, I. *Inorg. Chem.* **2002**, *41*, 5626.

(79) Vallet, V.; Wahlgren, U.; Grenthe, I. *J. Am. Chem. Soc.* **2003**, *125*, 14941.

(80) Flint, C. D.; Tanner, P. A. *Mol. Phys.* **1981**, *43*, 933.

(81) Mak, T. C. W.; Yip, W. H. *Inorg. Chim. Acta* **1985**, *109*, 131.

(82) Jones, L. H.; Penneman, R. A. *J. Chem. Phys.* **1953**, *21*, 542.

(83) Perron, H.; Roques, J.; Domain, C.; Drot, R.; Simoni, E.; Catalette, H. *Inorg. Chem.* **2008**, *47*, 10991.

(84) Valiev, M.; Garrett, B. C.; Tsai, M. K.; Kowalski, K.; Kathmann, S. M.; Schenter, G. K.; Dupuis, M. *J. Chem. Phys.* **2007**, 127.

(85) Milburn, G. H. W.; Truter, M. R. *J. Chem. Soc. A* **1966**, *1*, 1609.

(86) Guillaumont, R.; Fanghänel, T.; Grenthe, I.; Neck, V.; Palmer, D. A.; Rand, M. H. *Update on the Chemical Thermodynamics of Uranium, Neptunium, Plutonium, Americium and Technetium*; Elsevier: Amsterdam, The Netherlands, 2003; Vol. 5, p 970.